ROYAL SOCIETY OF CHEMISTRY

PAPER

Check for updates

Uncovering fast solid-acid proton conductors based on dynamics of polyanion groups and proton bonding strength†

Pjotrs Žguns, ‡[a] Konstantin Klyukin, ‡[ac] Louis S. Wang, [d] Grace Xiong, [d] Ju Li, [ab] Sossina M. Haile [d] and Bilge Yildiz *[ab]

Achieving high proton conductivity in inorganic solids is key for advancing many electrochemical technologies, including low-energy nano-electronics and energy-efficient fuel cells and electrolyzers. A quantitative understanding of the physical traits of a material that regulate proton diffusion is necessary for accelerating the discovery of fast proton conductors. In this work, we have mapped the structural, chemical and dynamic properties of solid acids to the elementary steps of the Grotthuss mechanism of proton diffusion. Our approach combines *ab initio* molecular dynamics simulations, analysis of phonon spectra and atomic structure calculations. We have identified the donor–hydrogen bond lengths and the acidity of polyanion groups as key descriptors of local proton transfer and the vibrational frequencies of the cation framework as the key descriptor of lattice flexibility. The latter facilitates rotations of polyanion groups and long-range proton migration in solid acid proton conductors. The calculated lattice flexibility also correlates with the experimentally reported superprotonic transition temperatures. Using these descriptors, we have screened the Materials Project database and identified potential solid acid proton conductors with monovalent, divalent and trivalent cations, including Ag^+, Sr^{2+}, Ba^{2+} and Er^{3+} cations, which go beyond the traditionally considered monovalent alkali cations (Cs^+, Rb^+, K^+, and NH_4^+) in solid acids.

Broader context

Discovery of fast proton conductors can significantly advance a wide range of technologies, including hydrogen fuel cells, electrolyzers, electrosynthesis of fuels, batteries and brain-inspired computing devices. Here, we identify promising fast proton conductors, focusing particularly on the class of solid acids, and go well beyond the traditionally considered chemistries. The key to this is having found physically based descriptors that map the structure and dynamics of the lattice to the atomistic mechanism of proton transport in solids, by leveraging computational tools, physical models, and extensive materials databases. These physical descriptors of proton conduction also provide paths for increasing the conductivity and decreasing the temperature of superprotonic transition. With the rapid growth of materials databases, our approach lays ground for the physically informed search of fast proton conductors and enlarges the chemical space of materials to power the green revolution.

a Department of Materials Science and Engineering, Massachusetts Institute of Technology, 77 Massachusetts Avenue, Cambridge, Massachusetts 02139, USA. E-mail: byildiz@mit.edu

b Department of Nuclear Science and Engineering, Massachusetts Institute of Technology, 77 Massachusetts Avenue, Cambridge, Massachusetts 02139, USA

c Department of Materials Engineering, Auburn University, Auburn, Alabama 36849, USA

d Department of Materials Science and Engineering, Northwestern University, Evanston, IL 60208, USA

† Electronic supplementary information (ESI) available. See DOI: https://doi.org/10.1039/d4ee01219d

‡ These authors contributed equally to this work.

Introduction

Inorganic solid electrolyte materials with high proton conductivity are important for advancing electrochemical devices for energy conversion, energy storage and energy-efficient computing, such as ceramic fuel cells and electrolyzers,[1–5] solid acid fuel cells,[6–8] hydrogen generators,[9] solid-state proton batteries,[10,11] electrochromic devices,[12] and magneto-ionic[13,14] and analog neuromorphic[15–18] computing hardware. Although high proton conductivities are reported for a range of material classes,[19–22] most of them show slow proton conductivity at low temperatures (*i.e.*, at room temperature), require special conditions such as a humid environment, or are not compatible with

5730 | *Energy Environ. Sci.*, 2024, **17**, 5730–5742

This journal is © The Royal Society of Chemistry 2024

particular technological standards. For example, state-of-the-art perovskite oxide ceramic electrolytes demonstrate sizable proton conductivity (10^{-3} S cm^{-1}) only above $\sim$300 °C.[22] At lower temperatures, proton diffusion in the bulk of perovskites is slow, and the reported room temperature conductivities are attributed to accumulated water interlayers, e.g., along grain boundaries or nanopores, rather than diffusion in the bulk lattice.[22] Metal–organic frameworks (MOFs)[23] and polymers such as Nafion[24] provide a conductivity of up to 10^{-2} S cm^{-1} at room temperature. These materials often require high humidity to conduct protons, and they are typically permeable to alcohols rendering them inapplicable for power generation using such fuels. Furthermore, they are incompatible with the processing of nanoelectronics using the complementary metal-oxide semiconductor (CMOS) technology. Novel solid-state proton conductors are sought after for near ambient-temperature applications. A quantitative understanding of the critical physical, structural, and chemical traits of a material that control proton conduction is necessary for developing the respective materials design strategies.

Solid acids constitute a promising class of proton conductors.[19,25] Solid acids are composed of metal cations and a network of polyanion groups (e.g., SeO$_4$, SO$_4$, and PO$_4$) that normally do not share corners or edges and are linked solely by hydrogen bonds. At low temperatures, the rigid hydrogen bonding network in solid acids results in low proton conductivities ($\sim$10^{-5} S cm^{-1}).[6,19] In the solid acids that exhibit high conductivities ($>10^{-3}$ S cm^{-1}), fast proton transport is achieved above the T_{sp} temperature of first-order, superprotonic transition (T_{sp} is typically within 100–300 °C).[6,19,25] The characteristic features of the superprotonic phase are facile rotation of polyanion groups (which even leads to their rotational disorder) and the accompanying dynamical disorder of hydrogen bond networks.[19,25] Both of these traits enable fast proton conduction via the Grotthuss mechanism[19,26] above the T_{sp} in solid acids. The rich compositional space available for solid acids allows tuning the properties of these compounds and potentially achieving high proton conductivity at lower temperatures.

High-throughput computational screening of materials is a promising approach for identifying fast proton conductors. Recently, extensive efforts have been devoted to screening solid-state Li-ions[27–34] and O-conductors,[34–36] allowing one to identify and experimentally verify promising solid-state electrolytes for the advancement of solid-state batteries and fuel cell technologies. The undertaken screening approaches can be broadly classified into three groups that use: (1) interpretable physical descriptors that are based on the ion diffusion mechanism,[29,33] (2) a data-driven approach to train machine learning models but not necessarily provide interpretable insights into the microscopic origin of why certain compounds are better ionic conductors than others,[27,30,35–37] and (3) high-throughput molecular dynamics (MD) simulations[28] to directly probe ionic diffusivities of screened compounds. Among the first two approaches, the first one that incorporates physical laws governing the microscopic diffusion mechanism into the

screening makes models more robust and interpretable and thus may be deemed superior[38] to the second one.

Computational screening for better proton conductors has been mostly limited to perovskites and related oxides.[36,39–41] It was found that the energy barriers for the covalent O–H bond rotation and proton transfer between acceptors and donors correlate with the energy of the O–H bond.[42] High-throughput studies of double-perovskites[40] and ternary oxides[41] revealed a correlation of the proton transfer barrier with the proton–acceptor distance, $d_{\text{H}\cdots\text{O}}$, as well as with the B-cation radius.[40] Another study demonstrated that oxygen affinity in the vicinity of dopants correlates positively with experimentally measured proton conductivities.[43] Recently developed machine learning models used experimental data to link extrinsic parameters such as temperature and chemical composition to proton concentrations in perovskite oxides,[36,39] without providing microscopic insights into the meaning of these extrinsic parameters. To the best of our knowledge, a search for physical descriptors and high throughput screening of proton-conducting electrolytes other than perovskites and related ceramic oxides have not been previously reported.

In this work, we consider materials that have hydrogen in their chemical formula and particularly examine the class of solid acids. We impose this limitation (that H is part of the structure) to focus on proton migration and its rate-limiting factors, without the need to consider the thermodynamics of proton incorporation. We first identify the physical descriptors of fast proton conduction in solid acids by establishing correlations between candidate descriptors and proton conductivities computed by means of ab initio molecular dynamics (AIMD) simulations. Next, we screen compounds from the Materials Project[44] database (that were also reported as existing under ambient conditions according to the ICSD[45] database) to select promising materials and then calculate their proton conductivity using machine-learning accelerated AIMD.[46–48] A detailed description of computational methods is available in Section S1 (ESI†). Through these methods we identify promising solid acid proton conductors containing cations outside of the traditionally considered monovalent alkali cation-based solid acids (Cs$^+$, Rb$^+$, K$^+$, and NH$_4^+$). These include the monovalent cations Ag$^+$ and Tl$^+$ as well as the divalent and trivalent cations such as Ba^{2+}, Sr^{2+} and Er^{3+}. In addition, we show that the descriptors of high proton conductivity, in particular lattice flexibility, may also be useful for predicting the transition temperature in known superprotonic conductors. Our work demonstrates that understanding the physical descriptors of the governing proton conduction mechanism can allow identification of new material candidates with rationally targeted properties.

Descriptors of the Grotthuss mechanism

The Grotthuss mechanism[19,25,26] is the underlying proton conduction mechanism in solid acids. It is broadly a two-step process (Fig. 1) involving: (i) proton transfer from donor to
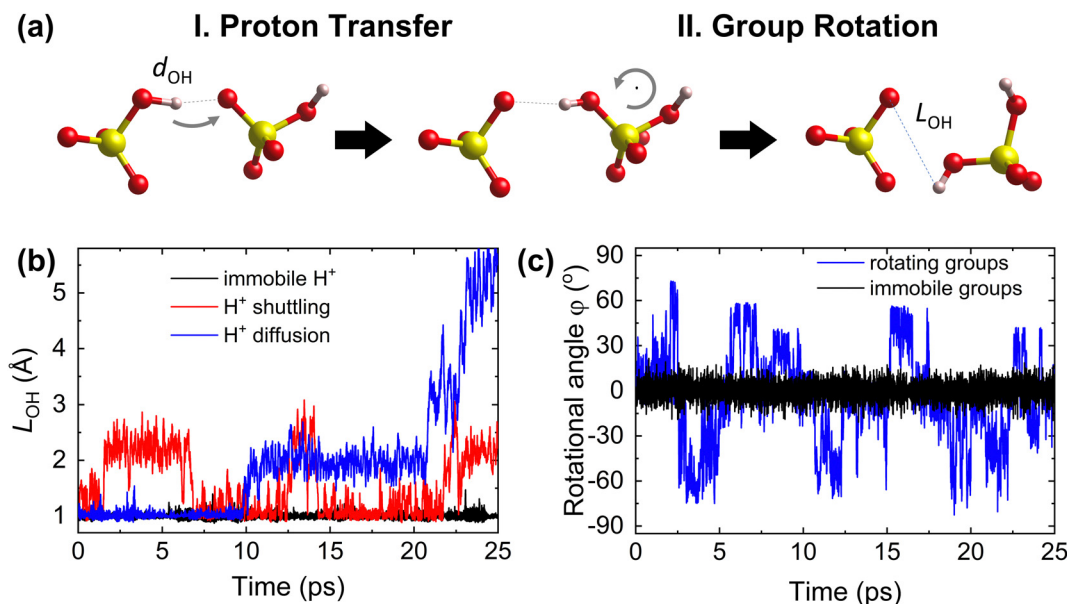
This journal is © The Royal Society of Chemistry 2024

Energy Environ. Sci., 2024, 17, 5730–5742 | 5731

Fig. 1 Steps of proton diffusion *via* the Grotthuss mechanism in a solid acid. (a) Donor and acceptor groups in a solid acid (yellow: S, red: O, and pink: H) Left: the proton is covalently bound to the initial donor (O on the left) and forms a hydrogen bond with the initial acceptor (O on the right). Middle: the proton has hopped and is covalently bound to the initial acceptor. Right: the acceptor group has rotated, taking the proton further away from the initial donor. (b) Time evolution of the proton–donor distance, L_{OH}, calculated from AIMD trajectories, showing three cases of proton transfer kinetics: an immobile proton, proton "shuttling" (confinement to back-and-forth motion between the same donor and acceptor), and long-range proton diffusion. (c) Time evolution of the azimuthal angle, φ, characterizing group rotation, where φ is defined within the internal coordinate system for each group vector (see Section S1 in the ESI†), calculated from AIMD simulations, showing two cases: rotationally immobile groups ($\varphi \approx 0°$) and rotationally mobile groups (displaying a large change of φ).

acceptor sites in which a covalent proton–donor bond is broken and a new covalent proton–acceptor bond is created and (ii) reorganization of the environment, specifically rotation of polyanion groups,[19,25,49] bringing the proton close to a new acceptor site and preventing a backward transfer to the original donor site.[19] For fast diffusion, the rates of both steps must be high. For example, slow or constrained rotation would confine protons to hopping mostly between the original donor and acceptor sites (Fig. 1). Below, we hypothesize descriptors of each step of the Grotthuss mechanism.

Proton transfer descriptors

Proton bonding to donor (D) and acceptor (A) atoms shows universal features. When the covalent D–H bond, d_{DH}, elongates, the hydrogen bond H···A, $d_{H···A}$, shrinks, and *vice versa*.[50] Moreover, the inverse relation between d_{DH} and $d_{H···A}$ is universal and holds well in various compounds.[19,50] This implies that the bond lengths d_{DH}, $d_{H···A}$ and d_{DA} are interdependent,[51] such that any one of them can be used as a descriptor of hydrogen bonding strength or proton transfer ease. The energy barrier for proton transfer grows with increasing transfer distance between acceptor and donor sites.[19] In molecular complexes, the proton transfer is nearly barrierless for $d_{OO} \approx 2.4$ Å and the barrier increases to about 1 eV for $d_{OO} \approx 3$ Å.[19,52] Similar relations of the proton transfer barrier to the donor–acceptor distances, d_{DA}, were shown for perovskite oxides,[53,54] solid acids[49] and ternary oxides.[41] We expect that the proton barrier dependence on the bond lengths is general for different compounds with O–H···O bonds.

Thus, we have assessed the covalent bond length, d_{DH}, as a descriptor of proton transfer in solid acids.

The energy barrier of proton transfer should similarly correlate with any other trait that reflects the D–H bond strength. For example, the acid dissociation constant, pK_a,[55–58] a common concept in liquid aqueous systems, reflects the extent of proton dissociation according to reaction: $H_3PO_4 + H_2O \rightarrow (H_2PO_4)^- + H_3O^+$, and we have assessed its relation to proton transfer in solid acids. Other possible descriptors include the bond stretching frequency[50] and bond order[50] or metrics that quantify the covalency of the donor–proton bond. The O 2p band center characterizes the covalence of bonds involving oxygen in metal oxides and is shown to correlate with the oxygen ion migration barrier[59] and hydrogen binding strength.[60] The position of O 2p states on the absolute energy scale was also found to correlate with proton affinity in closed-shell oxides.[61]

Group rotation descriptors

Rotational and network flexibilities are needed to enable the facile rotation of polyanion groups[19,25,49] to take the protons away from the vicinity of the original donor site. Superprotonic phase transition in solid acids is characterized by facile group rotations. This flexibility can be assessed from the lattice dynamics descriptors that reflect the rotational energy barrier. These include phonon band centers or phonon modes with a strong rotational character such as the so-called rigid unit modes.[62] Indeed, if rotational phonon modes of polyanion groups have a low frequency, one may expect[63] that the energy

barrier to group rotation is small. However, the identification of rotational modes of polyanion groups in solid acids and particularly their contribution to the Grotthuss mechanism is not trivial, as many modes may contribute to a rotational event. For high-throughput screening, we sought to describe the ease of rotation with a simple descriptor representing the most relevant modes. Along these lines, the force constants corresponding to octahedral rotations of low-frequency phonon modes were shown to correlate with oxygen anion interstitial migration barrier in Ruddlesden–Popper oxides.[64] Similarly, the average phonon band center of mobile Li-ion sites was found to correlate positively with their migration enthalpy.[63] The importance of the local structure[65] and lattice dynamics for proton[66] and hydrogen[67] conductivities was recently noted, and quantification of their role in proton conduction is desirable. For this purpose, as explained later, we have assessed the vibrational phonon modes of the framework cations as a proxy to the rotational flexibility of the polyanion groups.

Descriptors of group rotations may also be deduced from the topology of the hydrogen bonds or bonding constraints that rotating groups are subject to. For example, Maxwell has shown that frames (*e.g.*, made of struts and pins) are flexible if the number of degrees of freedom is larger than the number of constraints.[62,68] For solid acids, such analysis may include consideration of the number of bonds between the rotating groups and the rest of the crystal framework (*i.e.*, Cs–O in CsHSO$_4$). Although in solid acids the number of bonds can be very high (yet these "bonds" may be weak), they still develop exceptional rotational flexibility. Similarly, one may have to consider the topology of the hydrogen bonding network as it influences the rotations of polyanion groups.[19,25]

Summary of candidate descriptors

The complete set of hypothesized descriptors is summarized in Table 1. For proton transfer, we explicitly and quantitatively consider hydrogen bond lengths (both the covalent d_{OH} and the hydrogen bond $d_{H \cdots O}$), the acid dissociation constant, pK_a, and the O 2p band center position. The O–H stretching frequency was not assessed due to a higher computational cost as compared to d_{OH}. We did not find a generalizable correlation of the O 2p band center to the proton transport in our dataset (see Fig. S2 in the ESI†). While this could be due to various reasons, the relevant conclusion here is that the O 2p band center does not serve as a useful predictor of proton conductivity in solid acid materials. For rotational flexibility of the polyanion groups, we focused on the phonon modes of cations as a proxy, since the explicit assessment of the polyanion rotational modes and topological features was too complex to quantify across different structures and data sets.

Results and discussion

Descriptors of proton transfer

To test the proposed proton transfer descriptors (Table 1), we evaluated their correlation to the local metric of proton

Table 1 Hypothesized structural, chemical, and dynamic descriptors of the two steps of the Grotthuss mechanism of proton diffusion in inorganic solids in which the donor/acceptor is oxygen, O. The descriptors that were explored quantitatively in this work are marked with*

Descriptor	Property
Proton transfer	
d_{OH} (O–H bond length) (structural)*	O–H bond strength
$d_{H \cdots O}$ (H$\cdots$O distance) (structural)*	H-bonding network
pK_a (acid dissociation constant) (chemical)*	Dissociation ease
ω_{OH} (O–H stretching frequency) (dynamic)	O–H bond strength
O 2p band center (electronic)*	O–H bond strength
Rotational flexibility	
Phonon modes of polyanion groups (dynamic)	Lattice flexibility
Phonon modes of cations (dynamic)*	Lattice flexibility
Topological features, constraints (structural)	Structural reorganization

transfer, $L_{OH,max}$ (Fig. 1a and b) and the proton diffusivity, D_H, both extracted from AIMD simulations of 25 ps length at 700 K (see Section S1 in the ESI† for the comprehensive description of methods). $L_{OH} \approx 1.5$ Å is a typical mid-point between a donor and an acceptor. Thus, if $L_{OH,max} \lesssim 1.5$ Å, it can be concluded that the protons are immobile. Conversely, if 1.5 Å $\lesssim L_{OH,max} \lesssim 2$ Å, then proton transfer across the hydrogen bond occurred and if $L_{OH,max} \gtrsim 2$ Å, then the proton underwent additional diffusion (likely *via* polyanion group reorientation). Selecting $L_{OH,max} \approx 1.5$ Å defines a threshold metric for proton transfer, where larger values include both local proton transfer events and long-range proton diffusion.

The d_{OH} descriptor (defined as the largest of the O–H bond lengths in the initial structure; see Fig. 2a) showed a significant correlation with both $L_{OH,max}$ and D_H (Fig. 2b and c). All materials with a d_{OH} of > 1.007 Å demonstrated some proton transfer/diffusion, whereas materials with shorter O–H bonds demonstrated negligible transfer/diffusion. The ΔpK_a descriptor (the minimum absolute difference between the proton donor and acceptor group acidities) also showed a significant effect on both $L_{OH,max}$ and D_H (Fig. 2d and e). Nearly all materials with a ΔpK_a of < 5 demonstrated proton transfer/diffusion, whereas materials with larger ΔpK_a demonstrated negligible transfer/diffusion. Indeed, a large ΔpK_a value indicates that the energy difference between the acceptor and donor sites is large, which can increase the energy barrier.[69,70] The inherently low differences between the first and second and the second and third dissociation constants in sulfuric, phosphoric, arsenic, and selenic acids[58] are in agreement with fast local transport in superprotonic CsH$_2$PO$_4$,[71] CsH$_2$AsO$_4$,[71] CsHSO$_4$[72] and CsHSeO$_4$[72] and essentially indicate that the number of protons per polyanion group varies without incurring a high energy penalty, in support of the long-range proton transport. Among the two correlated descriptors (d_{OH} and ΔpK_a, see Fig. S3 in the ESI†), we expect that d_{OH} is more robust and accurate, encoding any structural/bonding variations in the solid that the tabulated pK_a values may not reflect. Therefore, we used d_{OH} in the final screening.

The data further show that the suggested criterion (d_{OH} > 1.007 Å) is necessary, but not sufficient, to identify fast

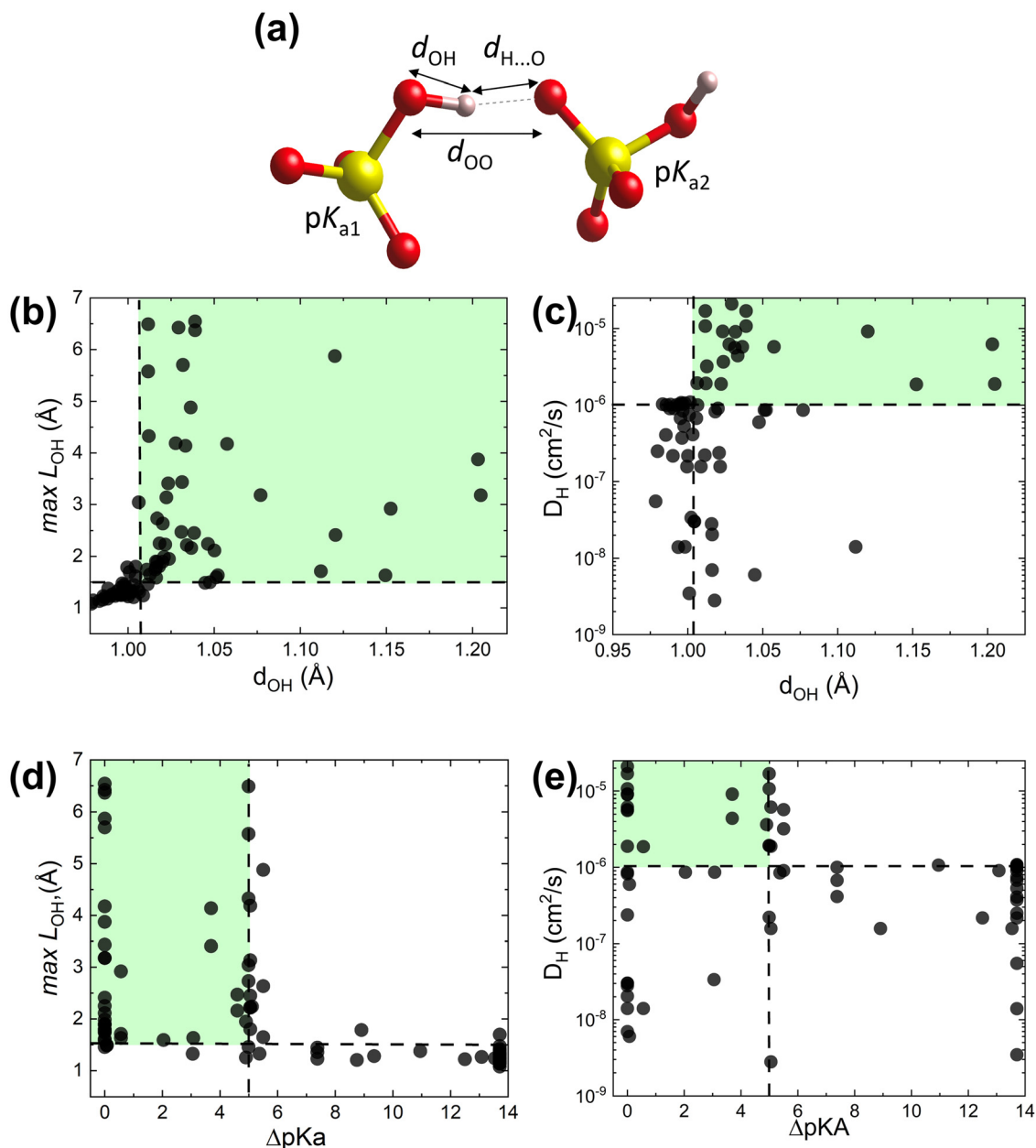This journal is © The Royal Society of Chemistry 2024

Energy Environ. Sci., 2024, **17**, 5730–5742 | **5733**

Fig. 2 AIMD results from the initial dataset to extract proton transfer descriptors. (a) Schematic showing d_{OH}, $d_{H\cdots O}$, d_{OO} and pK_a for donor and acceptor groups in a solid acid (color code: S is yellow, O is red, and H is pink). (b) Maximal distance travelled by the proton from its initial donor atom during the AIMD run, $L_{OH,max}$, vs. the maximal initial O–H bond length, d_{OH}. (c) Proton diffusivity, D_H vs. d_{OH}. (d) $L_{OH,max}$ vs. ΔpK_a. (e) D_H vs. ΔpK_a. All data at 700 K (the trajectory length is 25 ps). Dashed lines correspond to the selected cut-offs: D_H cut-off is set to 10^{-6} cm^2 s^{-1}, which corresponds to about 0.02 S cm^{-1} conductivity at 700 K and is above the AIMD accuracy limits (for further details see Computational methods, Section S1 in the ESI†).

conductors. Several examples of large d_{OH} materials show moderate values of $L_{OH,max}$ (~ 2 Å), Fig. 2b, and accordingly low diffusivities ($D_H < 10^{-6}$ cm^2 s^{-1}), Fig. 2c. Thus, by applying this criterion, we can filter out materials with a slow transfer rate (viz., poor conductors), but not every remaining material will be a fast proton conductor.

Descriptors of group rotation

As indicated in Table 1, we have hypothesized cation phonon modes to control the ease of rotational motion of polyanion groups. Accordingly, we analyzed the vibrational modes associated with group rotation and the flexibility of the lattice. We found that rotational modes of polyanion groups are often accompanied by pronounced displacements of the framework cations. This observation is consistent with arguments from the literature.[19] Fig. 3a shows the pattern of atomic displacements for a selected low-frequency phonon mode in CsHSO$_4$. Cs cations execute pronounced excursions during the SO$_4$ group rotation. The framework created by the cesium cations must be flexible to enable frequent and extensive rotations of polyanion
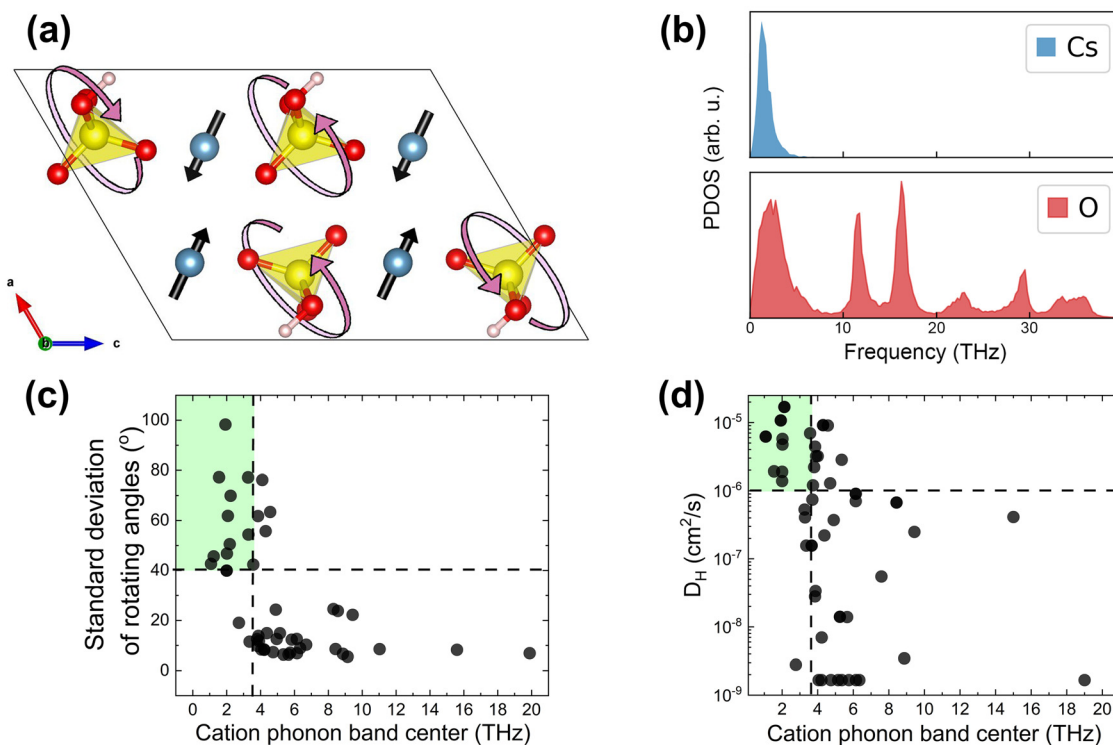
5734 | Energy Environ. Sci., 2024, **17**, 5730–5742

This journal is © The Royal Society of Chemistry 2024

Fig. 3 AIMD results from the initial dataset to extract group rotation descriptors. (a) Schematic of a low-frequency mode of SO_4 rotations accompanied by large displacements of Cs cations in $CsHSO_4$ (mp-1192419, $P2_1/c$;[73] Cs is blue, S is yellow, O is red, and H is pink). The SO_4 unit is largely intact, *i.e.*, the S–O bonds are not stretched during this rotation. (b) Cation and oxygen phonon density of states of $CsHSO_4$ (estimated as the power spectrum of the atomic velocities). (c) Rotational metric (the larger of the standard deviations of the polar and azimuthal angles, θ and φ, in spherical coordinates, characterizing group rotation, see Section S1 in the ESI†) *vs.* the cation phonon band center. (d) Proton diffusivity, D_H, *vs.* the cation phonon band center. Compounds that do not possess mono-oxyanion groups were excluded from analysis (Table S1, ESI†). All data at 700 K.

tetrahedra. Remarkably, the cesium phonon spectrum in $CsHSO_4$ has a peak only in the low-frequency range, as seen in Fig. 3b. This is because the cesium ions do not form strong covalent bonds and are largely "detached" from the stretching and bending modes of SO_4 polyanions. This means that the cation phonon band center (ω_{cat}) can serve as a proxy for all the low-frequency rotational modes in solid acids. Therefore, we use ω_{cat} as a descriptor of the lattice dynamic flexibility and the ease of the polyanion group rotations.

We define the rotational flexibility metric based on the standard deviations of the angles characterizing group rotations (*i.e.*, the polar and azimuthal angles, θ and φ, in the internal spherical coordinate system for each group vector, see Section S1 in the ESI†). We take the larger of the standard deviations of these two angles of rotation and show its dependence on the cation phonon band centers of the considered materials in Fig. 3c. The correlation between the proton diffusivity and the cation phonon band centers is shown in Fig. 3d. The majority of compounds with a low cation phonon band center (below about 3.5 THz) show good rotational flexibility, *i.e.* a large standard deviation of θ or φ, along with high proton diffusivity. For these compounds, the standard deviation of rotational angles is generally $\geq 40°$, indicating pronounced rotational excursions. This also means that 3 standard deviations correspond to about $120°$, which is comparable to the

$109.5°$ angle of the full tetrahedron rotation of the polyanion groups. Upon analyzing the maximal rotation angles observed during AIMD, a similar partition of compounds was found (Fig. S4, ESI†); *i.e.*, compounds that show full rotation of the polyanion tetrahedral with maximal rotational angles above $109.5°$ mostly have cation phonon band centers below 3.5 THz. Conversely, the majority of compounds with a high cation phonon band center (above about 3.5 THz) show poor rotational flexibility, with a rotational metric of lower than $40°$ (in fact, mostly lower than $40°$ as seen in Fig. 3c), and low diffusivity, indicating that the polyanion group rotation is limited. This correlation holds for all the compounds that we screened, except for a few that we excluded from consideration because the framework cations were partially or fully coordinated with water molecules (*e.g.*, $Nd(H_2O)_2(H_{0.5}SeO_3)_2$ and $Mg(H_2O)_6(SeO_3)$), which block correlated motion between the cation and the polyanion groups. Consequently, these compounds require a different metric to characterize the rotational motion of polyanion groups independent from the framework cations.[62,74]

Combining descriptors of proton transfer and group rotation

Since the Grotthuss mechanism is a two-step process, we considered separate descriptors for each step. One can see that individually each descriptor imposes a necessary but

insufficient condition for achieving a high diffusion coefficient for protons in solid acids. For example, the proton–donor bond length needs to be longer than a certain cut-off d_{OH} for proton transfer to take place (Fig. 2b and d), but this does not guarantee that diffusion will be long-range. Similarly, a low cation phonon band center favors good rotational flexibility, but it does not guarantee that proton transfer will be facile.

Fig. 4 shows a grouping of the simulated proton diffusion coefficients as a function of descriptors of both the proton transfer and the group rotation steps. We see that most of the fast proton conductors ($D_H^{700K} > 10^{-6}$ cm^2 s^{-1}, red data points in Fig. 4a) cluster in the region with a low cation phonon band center ($\lesssim 3.5$ THz) and a large initial O–H bond length ($d_{OH} \gtrsim 1.007$ Å). We observe a similar clustering in the ΔpK_a vs. ω_{cat} coordinates (Fig. 4b). The chosen cutoffs for ω_{cat} and d_{OH} allow us to separate proton conducting and non-conducting compounds with a low number of false-positive (3) and false-negative (4) cases. By using one descriptor each for proton transfer and for group rotation kinetics, we can predict which materials are expected to show both facile local proton hops and facile group rotation and therefore should be good proton conductors.

In summary, our results show that the length of the proton–donor covalent bond, d_{OH}, and the difference between donor and acceptor acidities, ΔpK_a, are good descriptors of the ease of proton transfer, and the cation phonon band center, ω_{cat}, is a good descriptor of the rotational flexibility of polyanion groups. Therefore, we next use these physically based descriptors to identify novel proton conductors by means of high-throughput computational screening. Between d_{OH} and ΔpK_a, we use the former in the high-throughput screening, as a more facile and structurally sensitive descriptor that we extract directly from the simulated structure in our calculations.

High-throughput screening based on physical descriptors

The screening workflow introduced in Computational methods (Section S1 in the ESI†) is detailed in Fig. 5. After an initial screening of 5207 materials based on various properties (steps I–IV), the dataset contained 874 compounds that possess low electronic conductivity, have hydrogen bonds, and are considered synthesizable. We have applied screening based on the identified descriptors on this data set of 874 compounds. Specifically, we selected materials that possess polyanion groups with a donor–hydrogen bond length, d_{OH}, longer than 1.007 Å (step V) and have a cation with the phonon band center, ω_{cat}, below 3.5 THz (step VI). Application of these criteria eliminated about 84% of materials that were not expected to be fast proton conductors, thus leaving 143 candidates (of which, 112 had unique compositions). The final dataset includes these 143 candidates. For these materials, we performed Machine Learning Force Field accelerated AIMD (MLFF–AIMD)[46–48] simulations to screen proton diffusivities at 650 K (step VII). We provide the complete list of materials, respective descriptors, and computed diffusivities in Table S2 (ESI†). Subsequently (step VIII), we selected the most promising compounds and explored their diffusivities in detail by MD (either AIMD or MLFF–AIMD) as a function of temperature below 650 K.

Before presenting the results of the diffusivity calculations, it is of value to consider the material properties of the 143 candidate conductors (Table S2, ESI†) treated in the final dataset. The majority of solid acids that satisfy the used criteria $d_{OH} > 1.007$ Å and $\omega_{cat} < 3.5$ THz are the Cs, Rb, and K-based ones (about 76%), and the rest are based on other cations including Ag^+, Hg^+, Tl^+, Ba^{2+}, Cd^{2+}, Pb^{2+}, Sr^{2+}, Er^{3+}, U^{6+} and Bi^{x+} (Fig. 6a). As evident in the scatter plot of features of these compounds, Fig. 6a, the d_{OH} values range from 1.007 Å to about 1.2 Å showing no preference across various elements or cation charges. In contrast, the ω_{cat} value broadly depends on the chemical element itself, leading to the formation of clusters of ω_{cat} values around each of Tl, Cs, Rb, Ag, Ba, and K-based compounds. The compound-averaged ω_{cat} values decrease as the effective cation radii increase (see Fig. S5, ESI†). This corroborates
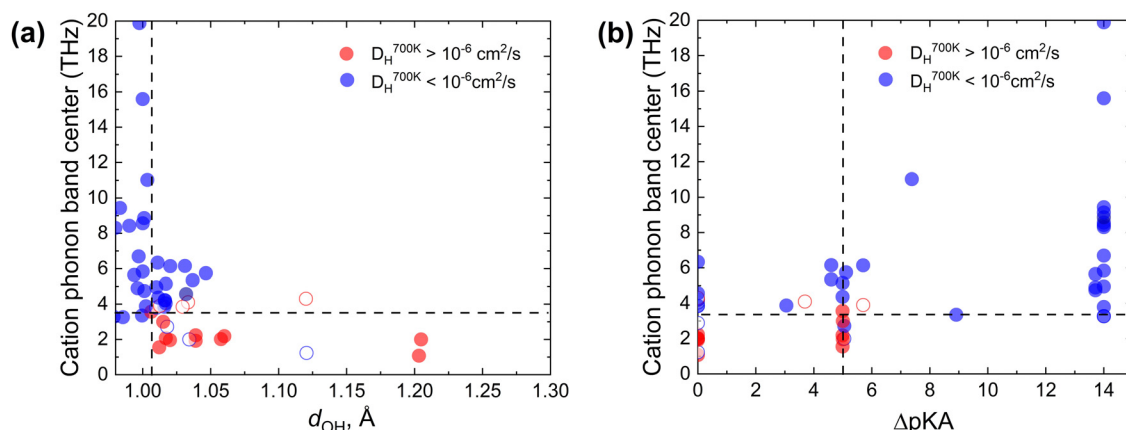

Fig. 4 (a) Scatter plot of D_H as a function of the cation phonon band center ω_{cat} and d_{OH}. Points are grouped/colored according to diffusivities from AIMD simulations at 700 K. Fast ($D_H > 10^{-6}$ cm^2 s^{-1}) proton conductors are shown in red, and slow ($D_H < 10^{-6}$ cm^2 s^{-1}) proton conductors are shown in blue. The clustering of fast proton conductors in the region with $d_{OH} \gtrsim 1.007$ Å and cation phonon band centers $\lesssim 3.5$ THz is seen. (b) The same as (a), but plotted in the ω_{cat} vs. ΔpK_a coordinates (a similar clustering of fast proton conductors is seen). Open circles highlight the false positive and false negative data points.
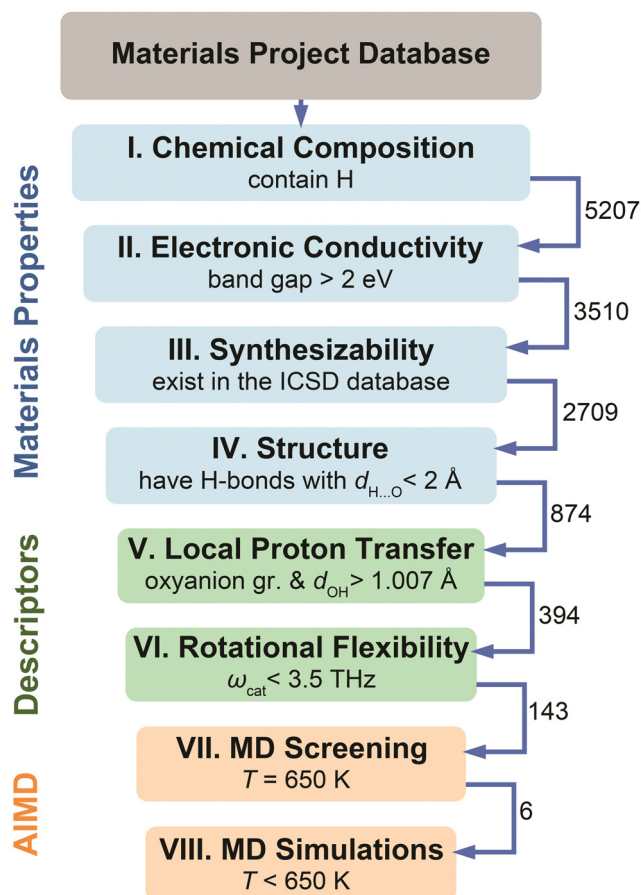
5736 | *Energy Environ. Sci.*, 2024, **17**, 5730–5742

This journal is © The Royal Society of Chemistry 2024

Fig. 5 Flowchart of the high-throughput screening of the Materials Project[44] database based on the materials properties (steps I–IV), the identified physical descriptors (steps V–VI), and MD diffusivities (steps VII–VIII). See Computational methods, Section S1 in the ESI,† for details regarding each step. The numbers near arrows show how many compounds reached the next step.

earlier hypotheses that large cations generally provide an increased lattice flexibility.[19,75] However, as can be seen in Fig. 6a, the cation size alone is not a sufficient condition for quantitatively relating to flexibility; *i.e.*, there is a range of ω_{cat} values for a group of compounds with the same cation. Different crystal structures with the same cation can have different flexibilities reflected with different cation phonon band centers. For example, Cs containing compounds have cation phonon band centers ranging from 1.2 THz to 2.7 THz. We also recognize that some compounds that passed the screening are toxic or radioactive, containing for example, Tl and U, and thus are not desirable for practical applications.

The computed diffusivities of the 143 compounds (from Fig. 6a and Table S2, ESI†) in the final dataset are presented as a histogram in Fig. 6b. About 30 compounds show high conductivity as evaluated at 650 K ($D_{H} \gtrsim 10^{-6}$ cm^2 s^{-1}; see discussion below regarding compounds with low conductivities). Importantly, our screening procedure finds most of the known Cs, Rb, and K-based compounds with superprotonic transitions, *e.g.*, $K_3H(SeO_4)_2$, $Rb_3H(SeO_4)_2$, $Cs_3H(SeO_4)_2$,

$CsHSO_4$, and $CsHSeO_4$,[6,76,77] which satisfy the proposed descriptor criteria and also demonstrate reasonable diffusivity in MD tests (see Table S2, ESI†). We also identify several less known Cs, Rb, and K-based compounds such as $Cs(HF)$-(H_2PO_4), $Rb(H_{2.5}AsO_4)_2$, and $K_4(H_3AsO_4)(HSO_4)_2(SO_4)$ that might be promising proton conductors (Table S2, ESI†).

We were particularly intrigued to find fast proton conductors among solid acids based on "unconventional" cations such as Ag^+, Ba^{2+}, Sr^{2+}, and Er^{3+}. We explored several such compounds using MD simulations as shown in Fig. 7 and summarized in Table 2. Their conductivities reach 10^{-2} S cm^{-1} at 500 K (Table 2), ranging from 10^{-3} to 10^{-1} S cm^{-1} between 400 and 600 K (Fig. 7). For example, $Er(HSO_4)_3$[78] shows 10^{-2} S cm^{-1} at 500 K and $Ag(H_3O)(HSO_4)_2$[79] shows 0.5 mS cm^{-1} at 400 K. The latter solid also supports vehicle diffusion, though it is a minor contribution to diffusion compared to the Grotthuss mechanism. Significantly, the calculated conductivities are higher than or comparable to that of $CsHSO_4$ (mp-1192419, $P2_1/c$ ref. 73) as shown in Fig. 7. To the best of our knowledge, the conductivities of these identified solid acids (Table 2 and Fig. 7) have not been experimentally reported in the literature.

In light of the low number of false positives indicated in Fig. 4, we were surprised that a large number of compounds passed our screening (Fig. 6a) but does not show fast proton diffusion at 650 K (Fig. 6b, Table S2, ESI†). There can be two reasons for this. First is that our screening criteria may be incomplete, and the screening model could be improved to filter out more of the non-conducting compounds by considering other factors, *e.g.*, the spatial arrangement of donor–acceptor sites and/or topology[84] of the hydrogen bonding network. In addition, some compounds have more than one cation, and we have screened based on only the one cation that has the ω_{cat} of <3.5 THz. For example, our dataset contained 40 solid acids that have more than one cation, such as $Ba_2Cd(H_{1.5}PO_4)_4$, $Ba_2CaH_6(PO_4)_4$, and $Ni_3AgH_2(PO_4)_3$, and the great majority of them showed negligible diffusion (Table S2, ESI†). All these compounds had another non-soft cation ($\omega_{cat} > 3.5$ THz), which can constrain the lattice flexibility. This is in agreement with our earlier experimental study that observed no superprotonic transition in $Cs_2Na(HSO_4)_3$ and $CsNa_2(HSO_4)_3$ and suggested that strong Na–O bonds hinder structural flexibility.[75]

A second reason for finding many of the screened compounds (from Fig. 6) with low proton diffusion at 650 K can be the use of the NVT ensemble in our MD simulations. By constraining the cell shape and volume, we do not allow explicit phase transitions (only rearrangements facilitated by temperature, see Fig. S6 and S7, ESI†). This constraint may suppress plausible superprotonic transitions and decrease diffusivity (*e.g.*, the simulated diffusivity of $CsHSO_4$ in Fig. 6 is by one order of magnitude lower than the experimental one,[6] and not every $CsHSO_4$ phase shows high diffusivity, see Table S2, ESI†). On the other hand, the predicted high conductivity does not guarantee that the phase will be stable at the simulated temperatures. For example, we predict triclinic[83] $Ba(H_2PO_4)_2$ to show exceptional conductivity (Fig. 7); however, this phase is

This journal is © The Royal Society of Chemistry 2024

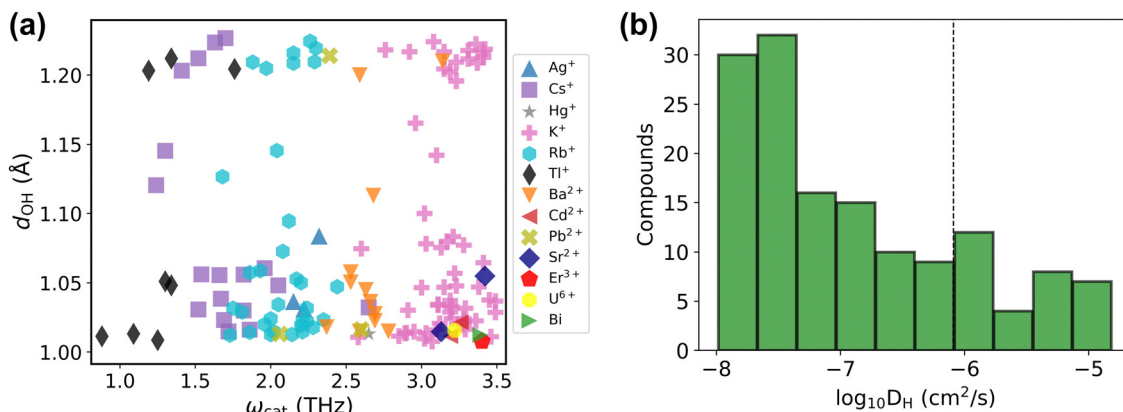*Energy Environ. Sci.*, 2024, **17**, 5730–5742 | **5737**

Fig. 6 Final dataset analysis. (a) The final dataset presented as the scatter plot of the maximal d_{OH} vs. cation phonon band center ω_{cat}. Different cations are highlighted with different colors (for compounds with multiple cations, the lowest ω_{cat} is plotted). The list of these compounds is provided in Table S2 (ESI†). (b) Histogram of diffusivities of the final dataset computed at 650 K using machine learning force field accelerated AIMD (MLFF–AIMD) simulations. The vertical dashed line marks $D_H \approx 10^{-6}$ cm^2 s^{-1}.
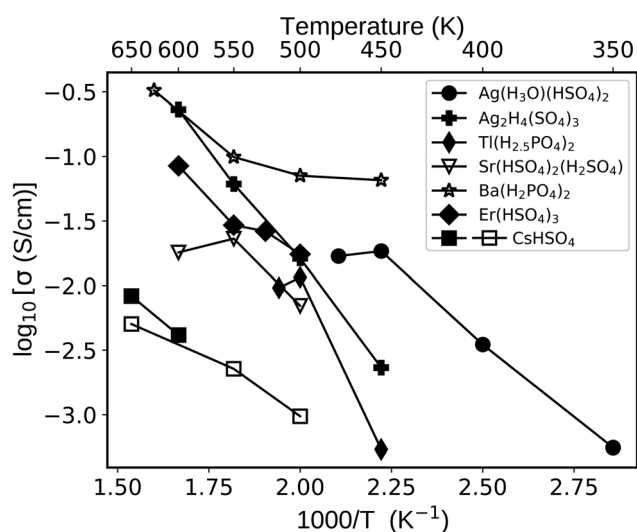

Fig. 7 Proton conductivities of selected solid acids calculated with AIMD (full symbols) and MLFF–AIMD (open symbols). The cell sizes and shapes were constrained to the room temperature (or low temperature) phases as retrieved from the Materials Project database (see Table 2). The simulated CsHSO$_4$ (mp-1192419) conductivity is shown as a baseline (MLFF–AIMD and AIMD demonstrate consistent results; see Section S1 in the ESI† for further details).

Table 2 The list of promising solid acids with non-Cs and non-Rb cations, their Materials Project[44] IDs, respective ICSD[45] IDs, and proton conductivities from our AIMD simulations shown in Fig. 7 (for Ba and Sr compounds, we used MLFF–AIMD). References to the experimental synthesis records from the ICSD are provided (all phases were reported at room temperature, except for the Sr compound reported at 160 K)

Compound	mp-ID	ICSD-ID	Ref.	σ_H (500 K) (mS cm^{-1})
Ag(H$_3$O)(HSO$_4$)$_2$[a]	mp-24072	408948	79	17 [@475 K]
Ag$_2$H$_4$(SO$_4$)$_3$[a]	mp-867593	408949	79	16
Tl(H$_{2.5}$PO$_4$)$_2$	mp-696762	30509	81	12
Sr(HSO$_4$)$_2$(H$_2$SO$_4$)[a]	mp-757723	404139	82	7
Ba(H$_2$PO$_4$)$_2$[b]	mp-706543	2420	83	70
Er(HSO$_4$)$_3$[a]	mp-24640	408804	78	17

[a] Hygroscopic, requires an inert atmosphere (see corresponding ref.)
[b] Meta-stable phase (triclinic) according to ref. 80.

the NVT ensemble, and explicit modelling of phase transitions would be desirable, yet challenging at present. Nevertheless, the calculated MD diffusivities (Table 2 and Fig. 7) remain strong indicators of fast proton conductivity in these compounds.

Our screening was limited to the Materials Project[44] database (about 154 thousand materials), yet more conductors may be identified by screening larger databases such as ICSD[45] (about 281 thousand compounds), OQMD[92] (about 1 million compounds), or GNoME (about 2.2 million compounds).[93] Rapid development of databases[93] and inverse materials design methods[38,94–97] presents an opportunity for such descriptor-based search of fast proton conductors with desirable properties (low T_{sp}, high chemical and thermal stabilities, etc.). In this regard, it is promising that our screening, albeit limited to the MP database, could uncover solid acids with less explored chemistries, demonstrating potential for screening of larger datasets[93] in future studies.

The established physical descriptors could be applied to other classes of proton conductors. However, such an expansion of the method requires considering the specifics of proton transfer and the Grotthuss reorganization of the environment,
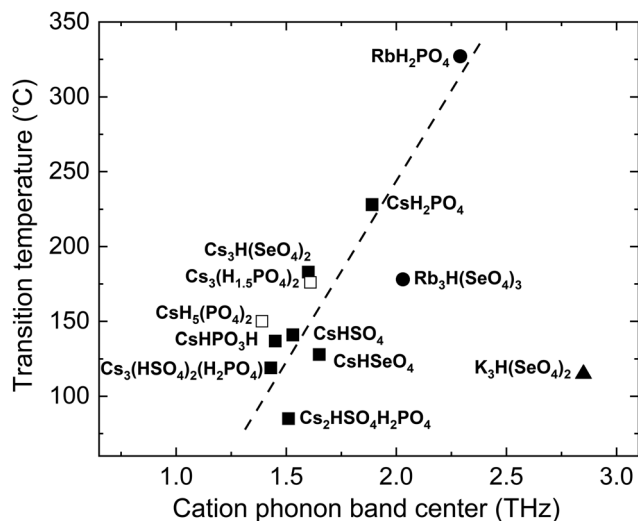
hard to stabilize.[80] The more stable orthorhombic phase does not show high proton conductivity either in experiments[85] or in our simulations (see mp-706400 record in Table S2, ESI†). Likewise, we cannot predict whether melting precedes[86,87] a superprotonic transition. Another limitation of the NVT ensemble is the assumption of a fixed stoichiometry and composition. However, in practice, proton conductivity in these compounds depends on the humidity and temperature, e.g., causing dehydration[88–90] or disproportionation,[91] both of which can affect conductivity. These examples of the behavior of Ba(H$_2$PO$_4$)$_2$ show that our MD diffusivities are influenced by

5738 | Energy Environ. Sci., 2024, **17**, 5730–5742

This journal is © The Royal Society of Chemistry 2024

Fig. 8 Experimental superprotonic transition temperature, T_{sp}, of solid acids from the literature *vs.* the average cation phonon band center, ω_{cat}, which is calculated in this work for each of those compounds. Open squares represent the melting temperatures of compounds that do not show superprotonic transition (*i.e.*, melt below an accessible T_{sp}). The trend line is the guide to the eye. Data points for Cs-based compounds[77,87,90,100–106] are squares, Rb-based compounds[77,103] are circles, and the K-based[77] solid acid is shown as a triangle.

and the chemistry and structure in each class of material, resulting in different quantitative relations of the descriptors to the conductivity. Possible classes include but are not limited to perovskites and other ceramic oxides[22] as well as polymer conductors.[24] For example, in metal oxides, while we do not expect significant rotations of the metal–oxygen polyhedra (as opposed to the rotations of polyanion groups in solid acids), we can expect that the lattice flexibility can still play a role by dynamically bringing closer donor–acceptor pairs assisted by different phonon modes at finite temperatures. Similar design principles, such as searching for complex compounds with a continuous hydrogen bonding network as in the newly discovered $ZrH_5(PO_4)_3$ solid acid,[98] provide another promising route to find fast, solid-state proton conductors.

Superprotonic transition temperature and its correlation with cation phonon band centers

For superprotonic solid acids, it is imperative to know not only whether a high conductivity phase exists, but also the temperature above which the high conductivity phase is stable, *i.e.*, the superprotonic transition temperature, T_{sp}. It is desirable to obtain materials with relatively low T_{sp} such that the superprotonic phase is encountered prior to melting or dehydration.[99] To address this, we explored correlations between T_{sp} and the descriptor of group rotation flexibility. The rationale is that the polyanion sublattice "rotationally melts" in the superprotonic phase; therefore, T_{sp} should correlate with the rotational flexibility and descriptors thereof.

We found that the experimentally measured T_{sp} in a comprehensive set of Cs-containing superprotonic solid acids correlates with the calculated cation phonon band center, Fig. 8.

For compounds with multiple, inequivalent Cs sites, which display distinct band centers for each unique Cs (*e.g.*, Cs_2HSO_4-H_2PO_4 [1.43 THz and 1.60 THz] and $Cs_3(HSO_4)_2(H_2PO_4)$ [1.36 THz, 1.50 THz, 1.81 THz]), we used the average frequencies from different cation sites. The greater the flexibility of the cation framework under ambient conditions, the lower the temperature required for transitioning to the superprotonic phase. This observed correlation implies that the superprotonic transition in these materials is indeed related to the rotational flexibility of polyanion groups. However, the rotational flexibility may alternatively lead to a complete melting transition, as is the case for two of the nine compounds considered, and additional criteria will be required to distinguish between the type of transition that occurs. Significantly, two identified Rb superprotonic compounds fall along the same trend line with the Cs compounds, reflecting chemical similarity between these species. The representative K compound indicated in Fig. 8 deviates from the trend line. Because there are a very limited number of experimental reports of superprotonic phase transition in solid acids that do not include Cs, the possibilities for elucidating the specific role of the cation species are limited, though cation mass may directly play a role by affecting the force constants (Fig. S8, ESI†).

Dependence of T_{sp} on the softness of the cation framework underscores the importance of lattice flexibility. A large cation size alone is not a sufficient quantitative indicator of increased lattice flexibility and the lowering of T_{sp}. As seen in Fig. 8, even for solid acids with the same framework cation, Cs, T_{sp} varies more than 100 °C and the ω_{cat} varies by about 1 THz. Explicit quantification of lattice flexibility (*i.e.*, through the cation phonon band center, as done here) appears to be a more useful predictor of T_{sp}. Since the correlation between ω_{cat} and T_{sp} is not precise, consideration of other factors, for example, bonding network topology, inequivalence of cation sites and the role of multiple phonon band centers, and disparity of the cation masses, may provide further insights into the complete set of factors that control T_{sp}.

Conclusion

In this work, we have established quantitative conditions for physical descriptors that enable high proton conductivity in solid acids. The physical descriptors correspond to the two key steps of proton transport based on the Grotthuss mechanism. The ease of proton transfer between the donor and acceptor sites depends on the donor–proton (O–H) bond strength, inversely related to the bond length d_{OH}; *i.e.*, larger d_{OH} leads to easier local proton transfer. Similarly, the smaller the difference in pK_a of the donor and acceptor sites, the easier the local proton transfer. The rotational flexibility of the polyanion groups depends on the phonon band center of the framework cation sublattice, ω_{cat}; *i.e.*, lower ω_{cat} leads to a softer cation framework, a more flexible lattice and easier group rotations. The cation phonon band center also correlates with the experimentally reported temperatures of superprotonic

This journal is © The Royal Society of Chemistry 2024

Energy Environ. Sci., 2024, **17**, 5730–5742 | **5739**

transition. This finding suggests that increasing the lattice flexibility to facilitate polyanion group rotations can decrease T_{sp} and help achieve high proton conductivity at lower temperatures. Our work provides guidance on how to quantify the rotational flexibility and T_{sp} based on the lattice dynamics features for arbitrary compositions. The model for descriptors of proton conductivity and T_{sp} can be further improved in the future to include other possible factors, such as the network topology of hydrogen bonds and structural constraints on the group rotations.

Based on the identified descriptors, we screened the Materials Project[44] database and revealed potential solid acid proton conductors. The well-known fast proton conductors with Cs^+, Rb^+, and K^+ framework cations satisfy our descriptor criteria. We also found prospective fast proton conductors with "unconventional" cations for solid acid proton conductors. These include Ag^+, Ba^{2+}, Sr^{2+} and Er^{3+} framework cations. AIMD simulations indicate that these compounds can possess proton conductivities that are higher than that of $CsHSO_4$. This finding of "unconventional" chemistries suggests that there is an opportunity to reveal more solid acid proton conductors by screening larger materials databases. We expect that the available compositional space of proton-conducting solid acids is broader than what has been used so far. We believe that our results will inspire further studies to investigate larger materials datasets and implement novel proton-conducting solid acids for different applications from energy conversion to electronic devices.

Data availability

The data supporting this article have been included as part of the ESI.†

Conflicts of interest

There are no conflicts to declare.

Acknowledgements

References

1 C. Duan, J. Tong, M. Shang, S. Nikodemski, M. Sanders, S. Ricote, A. Almansoori and R. O'Hayre, *Science (1979)*, 2015, **349**, 1321–1326.

2 S. Choi, C. J. Kucharczyk, Y. Liang, X. Zhang, I. Takeuchi, H.-I. Ji and S. M. Haile, *Nat. Energy*, 2018, **3**, 202–210.

3 H. An, H. W. Lee, B. K. Kim, J. W. Son, K. J. Yoon, H. Kim, D. Shin, H. Il Ji and J. H. Lee, *Nat. Energy*, 2018, **3**, 870–875.

4 H. Ding, W. Wu, C. Jiang, Y. Ding, W. Bian, B. Hu, P. Singh, C. J. Orme, L. Wang, Y. Zhang and D. Ding, *Nat. Commun*, 2020, **11**, 1907.

5 F. Liu, H. Deng, H. Ding, P. Kazempoor, B. Liu and C. Duan, *Joule*, 2023, **7**, 1308–1332.

6 S. M. Haile, D. A. Boysen, C. R. I. Chisholm and R. B. Merie, *Nature*, 2001, **410**, 910–913.

7 D. A. Boysen, T. Uda, C. R. I. Chisholm and S. M. Haile, *Science (1979)*, 2004, **303**, 68–70.

8 T. Uda, D. A. Boysen, C. R. I. Chisholm and S. M. Haile, *Electrochem. Solid-State Lett.*, 2006, **9**, A261–A264.

9 D. K. Lim, A. B. Plymill, H. Paik, X. Qian, S. Zecevic, C. R. I. Chisholm and S. M. Haile, *Joule*, 2020, **4**, 2338–2347.

10 X. Wu, J. J. Hong, W. Shin, L. Ma, T. Liu, X. Bi, Y. Yuan, Y. Qi, T. W. Surta, W. Huang, J. Neuefeind, T. Wu, P. A. Greaney, J. Lu and X. Ji, *Nat. Energy*, 2019, **4**, 123–130.

11 L. Yan, J. Huang, Z. Guo, X. Dong, Z. Wang and Y. Wang, *ACS Energy Lett.*, 2020, 685–691.

12 Z. Shao, A. Huang, C. Ming, J. Bell, P. Yu, Y.-Y. Sun, L. Jin, L. Ma, H. Luo, P. Jin and X. Cao, *Nat. Electron.*, 2022, **5**, 1–8.

13 A. J. Tan, M. Huang, C. O. Avci, F. Büttner, M. Mann, W. Hu, C. Mazzoli, S. Wilkins, H. L. Tuller and G. S. D. Beach, *Nat. Mater.*, 2019, **18**, 35–41.

14 M. Huang, M. U. Hasan, K. Klyukin, D. Zhang, D. Lyu, P. Gargiani, M. Valvidares, S. Sheffels, A. Churikova, F. Büttner, J. Zehner, L. Caretta, K. Y. Lee, J. Chang, J. P. Wang, K. Leistner, B. Yildiz and G. S. D. Beach, *Nat. Nanotechnol.*, 2021, **16**, 981–988.

15 X. Yao, K. Klyukin, W. Lu, M. Onen, S. Ryu, D. Kim, N. Emond, I. Waluyo, A. Hunt, J. A. del Alamo, J. Li and B. Yildiz, *Nat. Commun.*, 2020, **11**, 3134.

16 M. Onen, N. Emond, J. Li, B. Yildiz and J. A. Del Alamo, *Nano Lett.*, 2021, **21**, 6111–6116.

17 M. Onen, N. Emond, B. Wang, D. Zhang, F. M. Ross, J. Li, B. Yildiz and J. A. del Alamo, *Science (1979)*, 2022, **377**, 539–543.

18 M. Huang, M. Schwacke, M. Onen, J. del Alamo, J. Li and B. Yildiz, *Adv. Mater.*, 2022, 2205169.

19 K.-D. Kreuer, *Chem. Mater.*, 1996, **8**, 610–641.

20 T. Norby, *Solid State Ionics*, 1999, **125**, 1–11.

21 L. Malavasi, C. A. J. Fisher and M. S. Islam, *Chem. Soc. Rev.*, 2010, **39**, 4370–4387.

22 Y. Meng, J. Gao, Z. Zhao, J. Amoroso, J. Tong and K. S. Brinkman, *J. Mater. Sci.*, 2019, **54**, 9291–9312.

23 K. Biradha, A. Goswami, R. Moi and S. Saha, *Dalton Trans.*, 2021, **50**, 10655–10673.

5740 | *Energy Environ. Sci.*, 2024, **17**, 5730–5742

This journal is © The Royal Society of Chemistry 2024

24 Y. Sone, P. Ekdunge and D. Simonsson, *J. Electrochem. Soc.*, 1996, **143**, 1254–1259.

25 A. I. Baranov, *Crystallogr. Rep.*, 2003, **48**, 1012–1037.

26 K. D. Kreuer, *Solid State Ionics*, 1997, **94**, 55–62.

27 Y. Zhang, X. He, Z. Chen, Q. Bai, A. M. Nolan, C. A. Roberts, D. Banerjee, T. Matsunaga, Y. Mo and C. Ling, *Nat. Commun.*, 2019, **10**, 1–7.

28 L. Kahle, A. Marcolongo and N. Marzari, *Energy Environ. Sci.*, 2020, **13**, 928–948.

29 S. Muy, J. Voss, R. Schlem, R. Koerver, S. J. Sedlmaier, F. Maglia, P. Lamp, W. G. Zeier and Y. Shao-Horn, *iScience*, 2019, **16**, 270–282.

30 A. D. Sendek, E. D. Cubuk, E. R. Antoniuk, G. Cheon, Y. Cui and E. J. Reed, *Chem. Mater.*, 2019, **31**, 342–352.

31 B. He, P. Mi, A. Ye, S. Chi, Y. Jiao, L. Zhang, B. Pu, Z. Zou, W. Zhang, M. Avdeev, S. Adams, J. Zhao and S. Shi, *Acta Mater*, 2021, **203**, 116490.

32 B. He, S. Chi, A. Ye, P. Mi, L. Zhang, B. Pu, Z. Zou, Y. Ran, Q. Zhao, D. Wang, W. Zhang, J. Zhao, S. Adams, M. Avdeev and S. Shi, *Sci Data*, 2020, **7**, 1–14.

33 K. J. Jun, Y. Sun, Y. Xiao, Y. Zeng, R. Kim, H. Kim, L. J. Miara, D. Im, Y. Wang and G. Ceder, *Nat. Mater.*, 2022, **21**, 924–931.

34 C. López, A. Emperador, E. Saucedo, R. Rurali and C. Cazorla, *Mater. Horiz.*, 2023, **10**, 1757–1768.

35 M. Matsubara, A. Suzumura, N. Ohba and R. Asahi, *Commun. Mater.*, 2020, **1**, 1–6.

36 P. Priya and N. R. Aluru, *npj Comput. Mater.*, 2021, **7**, 1–12.

37 A. D. Sendek, Q. Yang, E. D. Cubuk, K. A. N. Duerloo, Y. Cui and E. J. Reed, *Energy Environ. Sci.*, 2017, **10**, 306–320.

38 K. E. Willcox, O. Ghattas and P. Heimbach, *Nat. Comput. Sci.*, 2021, **1**, 166–168.

39 J. Hyodo, K. Tsujikawa, M. Shiga, Y. Okuyama and Y. Yamazaki, *ACS Energy Lett.*, 2021, **6**, 2985–2992.

40 M. S. Islam, S. Wang, A. M. Nolan and Y. Mo, *Chem. Mater.*, 2021, **33**, 8278–8288.

41 M. S. Islam, S. Wang, A. T. Hall and Y. Mo, *Chem. Mater.*, 2022, **34**, 5938–5948.

42 N. Bork, N. Bonanos, J. Rossmeisl and T. Vegge, *Phys. Rev. B: Condens. Matter Mater. Phys.*, 2010, **82**, 014103.

43 Y. Yamazaki, A. Kuwabara, J. Hyodo, Y. Okuyama, C. A. J. Fisher and S. M. Haile, *Chem. Mater.*, 2020, **32**, 7292–7300.

44 A. Jain, S. P. Ong, G. Hautier, W. Chen, W. D. Richards, S. Dacek, S. Cholia, D. Gunter, D. Skinner, G. Ceder and K. A. Persson, *APL Mater.*, 2013, **1**, 011002.

45 A. Belkly, M. Helderman, V. L. Karen and P. Ulkch, *Acta Crystallogr., Sect. B: Struct. Sci.*, 2002, **58**, 364–369.

46 R. Jinnouchi, J. Lahnsteiner, F. Karsai, G. Kresse and M. Bokdam, *Phys. Rev. Lett.*, 2019, **122**, 225701.

47 R. Jinnouchi, F. Karsai and G. Kresse, *Phys. Rev. B*, 2019, **100**, 14105.

48 R. Jinnouchi, F. Karsai, C. Verdi, R. Asahi and G. Kresse, *J. Chem. Phys.*, 2020, **152**, 234102.

49 C. Dreßler and D. Sebastiani, *Phys. Chem. Chem. Phys.*, 2020, **22**, 10738–10752.

50 T. Steiner, *Angew. Chem., Int. Ed.*, 2002, **41**, 48–76.

51 M. Ichikawa, *Acta Crystallogr., Sect. B: Struct. Crystallogr. Cryst. Chem.*, 1978, **34**, 2074–2080.

52 D. Borgis, G. Tarjus and H. Azzouz, *J. Chem. Phys.*, 1992, **97**, 1390–1400.

53 W. Münch, G. Seifert, K. D. Kreuer and J. Maier, *Solid State Ionics*, 1997, **97**, 39–44.

54 M. F. Hoedl, A. Chesnokov, D. Gryaznov, R. Merkle, E. A. Kotomin and J. Maier, *J. Mater. Chem. A*, 2023, **11**, 6336–6348.

55 D. A. Evans and D. H. Ripin, "pKa's of Inorganic and Oxo-Acids," can be found under https://www.wanglab.chem.pitt.edu/wp-content/uploads/2017/09/Evans-D.-A.-Ripin-D.-H.-The-Evans-pKa-Table-Harvard-2006.pdf.

56 C. J. Peacock and G. Nickless, *Z. Naturforsch., A: Phys. Sci.*, 1969, **24**, 245–247.

57 "Engineering ToolBox, (2017), Inorganic Acids and Bases – pKa Values.," can be found under https://www.engineeringtoolbox.com/pKa-inorganic-acid-base-hydrated-metal-ion-monoprotic-diprotic-triprotic-tetraprotic-d_1950.html.

58 W. M. Haynes, ed., *CRC Handbook of Chemistry and Physics*, Taylor & Francis, 2014.

59 T. T. Mayeshiba and D. D. Morgan, *Solid State Ionics*, 2016, **296**, 71–77.

60 C. F. Dickens, J. H. Montoya, A. R. Kulkarni, M. Bajdich and J. K. Nørskov, *Surf. Sci.*, 2019, **681**, 122–129.

61 T. S. Bjørheim, M. F. Hoedl, R. Merkle, E. A. Kotomin and J. Maier, *J. Phys. Chem. C*, 2020, **124**, 1277–1284.

62 M. T. Dove, *Philos. Trans. R. Soc., A*, 2019, 377, DOI: 10.1098/RSTA.2018.0222.

63 S. Muy, J. C. Bachman, L. Giordano, H. H. Chang, D. L. Abernathy, D. Bansal, O. Delaire, S. Hori, R. Kanno, F. Maglia, S. Lupart, P. Lamp and Y. Shao-Horn, *Energy Environ. Sci.*, 2018, **11**, 850–859.

64 X. Li and N. A. Benedek, *Chem. Mater.*, 2015, **27**, 2647–2652.

65 A. Torayev, L. Sperrin, M. A. Gomez, J. A. Kattirtzi, C. Merlet and C. P. Grey, *J. Phys. Chem. C*, 2020, **124**, 16689–16701.

66 T. Itakura, H. Matsui, T. Tada, S. Kitagawa, A. Demessence and S. Horike, *Chem. Sci.*, 2020, **11**, 1538–1541.

67 V. Korostelev, J. Wagner and K. Klyukin, *J. Mater. Chem. A*, 2023, **11**, 23576–23588.

68 J. C. Maxwell, *London, Edinburgh Dublin Philos. Mag. J. Sci.*, 1864, **27**, 294–299.

69 R. P. Bell, *Proc. R. Soc. London*, 1936, **154**, 414–429.

70 M. G. Evans and M. Polanyi, *Trans. Faraday Soc.*, 1936, **32**, 1333–1360.

71 A. I. Baranov, V. P. Khiznichenko and L. A. Shuvalov, *Ferroelectrics*, 1989, **100**, 135–141.

72 A. I. Baranov, L. A. Shuvalov and N. M. Shchagina, *JETP Lett.*, 1982, **36**, 459–462.

73 K. Itoh, T. Ukeda, T. Ozaki and E. Nakamura, IUCr, *Acta Crystallogr.*, 1990, **C46**, 358–361.

74 M. T. Dove, J. Du, Z. Wei, D. A. Keen, M. G. Tucker and A. E. Phillips, *Phys. Rev. B*, 2020, **102**, 094105.

75 C. R. I. Chisholm, L. A. Cowan and S. M. Haile, *Chem. Mater.*, 2001, **13**, 2909–2912.

76 A. Goñi-Urtiaga, D. Presvytes and K. Scott, *Int. J. Hydrogen Energy*, 2012, **37**, 3358–3372.

This journal is © The Royal Society of Chemistry 2024

Energy Environ. Sci., 2024, **17**, 5730–5742 | 5741

77 D. Yi, S. Sanghvi, C. P. Kowalski and S. M. Haile, *Chem. Mater.*, 2019, **31**, 9807–9818.

78 M. S. Wickleder, *Z. Anorg. Allg. Chem.*, 1998, **624**, 1347–1354.

79 A. Stiewe, E. Kemnitz and S. Troyanov, *Z. Anorg. Allg. Chem.*, 1999, **625**, 329–335.

80 B. Prelesnik, R. Herak, M. Čurić and I. Krstanović, *Acta Crystallogr.*, 1978, **34**, 76–78.

81 Y. Oddon, J.-R. Vignalou, A. Tranquard and G. Pèpe, *Acta Crystallogr.*, 1978, **34**, 3510–3514.

82 C. Werner, E. Kemnitz, H. Worzala and S. Trojanov, *Z. Naturforsch., B: J. Chem. Sci.*, 1996, **51**, 952–958.

83 J. D. Gilbert and P. G. Lenhert, *Acta Crystallogr.*, 1978, **34**, 3309–3312.

84 K. S. Gomez-Haibach and M. A. Gomez, *J. Phys. Chem. B*, 2023, **127**, 9258–9266.

85 I. N. Bagryantseva and V. G. Ponomareva, *Inorg. Mater.*, 2018, **54**, 366–373.

86 S. Chandrasekhar, R. Shashidhar and N. Tara, *Mol. Cryst. Liq. Cryst.*, 1970, **10**, 337–358.

87 G. V. Lavrova, E. B. Burgina, A. A. Matvienko and V. G. Ponomareva, *Solid State Ionics*, 2006, **177**, 1117–1122.

88 S. M. Haile, C. R. I. Chisholm, K. Sasaki, D. A. Boysen and T. Uda, *Faraday Discuss.*, 2006, **134**, 17–39.

89 Y. K. Taninouchi, T. Uda, Y. Awakura, A. Ikeda and S. M. Haile, *J. Mater. Chem.*, 2007, **17**, 3182–3189.

90 A. Ikeda and S. M. Haile, *Solid State Ionics*, 2012, **213**, 63–71.

91 L. A. Cowan, R. M. Morcos, N. Hatada, A. Navrotsky and S. M. Haile, *Solid State Ionics*, 2008, **179**, 305–313.

92 S. Kirklin, J. E. Saal, B. Meredig, A. Thompson, J. W. Doak, M. Aykol, S. Rühl and C. Wolverton, *NPJ Comput Mater*, 2015, **1**, 15010.

93 A. Merchant, S. Batzner, S. S. Schoenholz, M. Aykol, G. Cheon and E. D. Cubuk, *Nature*, 2023, **624**, 80–85.

94 B. Sanchez-Lengeling and A. Aspuru-Guzik, *Science (1979)*, 2018, **361**, 360–365.

95 V. Fung, J. Zhang, G. Hu, P. Ganesh and B. G. Sumpter, *npj Comput. Mater.*, 2021, **7**, 200.

96 Z. Ren, S. I. P. Tian, J. Noh, F. Oviedo, G. Xing, J. Li, Q. Liang, R. Zhu, A. G. Aberle, S. Sun, X. Wang, Y. Liu, Q. Li, S. Jayavelu, K. Hippalgaonkar, Y. Jung and T. Buonassisi, *Matter.*, 2022, **5**, 314–335.

97 M. A. Q. Microsoft Research AI4Science, https://arxiv.org/abs/2311.07361, 2023.

98 S. Fop, R. Vivani, S. Masci, M. Casciola and A. Donnadio, *Angew. Chem.,– Int. Ed.*, 2023, **62**, e2022184.

99 S. Chandrasekhar, R. Shashidhar and N. Tara, *Mol. Cryst. Liq. Cryst.*, 1970, **10**, 337–358.

100 Z. Jiráak, M. Dlouhá, S. Vratislav, A. M. Balagurov, A. I. Beskrovnyi, V. I. Gordelii, I. D. Datt and L. A. Shwalov, *Phys. Status Solidi A*, 1987, **100**, K117–K122.

101 S. M. Haile, G. Lentz, K. D. Kreuer and J. Maier, *Solid State Ionics*, 1995, **77**, 128–134.

102 M. A. Zakharov, S. I. Troyanov and E. Kemnitz, *Z. Kristallogr.*, 2001, **216**, 172–175.

103 D. A. Boysen, S. M. Haile, H. Liu and R. A. Secco, *Chem. Mater.*, 2003, **15**, 727–736.

104 S. Sanghvi and S. M. Haile, *Solid State Ionics*, 2020, **349**, 115291.

105 C. R. I. Chisholm, R. B. Merle, D. A. Boysen and S. M. Haile, *Chem. Mater.*, 2002, **14**, 3889–3893.

106 C. R. I. Chisholm and S. M. Haile, *Solid State Ionics*, 2000, **136–137**, 229–241.

5742 | *Energy Environ. Sci.*, 2024, **17**, 5730–5742

This journal is © The Royal Society of Chemistry 2024